Recombinant Protein-Stabilized Monodisperse Microbubbles with Tunable Size Using a Valve-Based Microfluidic Device

Francesco E. Angilè,[†] Kevin B. Vargo,[†] Chandra M. Sehgal,[§] Daniel A. Hammer,[†,‡] and Daeyeon Lee*[,†]

[†]Department of Chemical and Biomolecular Engineering and [‡]Department of Bioengineering, School of Engineering and Applied Science, University of Pennsylvania, Philadelphia, Pennsylvania 19104, United States

[§]Department of Radiology, University of Pennsylvania Medical Center, Philadelphia, Pennsylvania 19104, United States

 Supporting Information

ABSTRACT: Microbubbles are used as contrast enhancing agents in ultrasound sonography and more recently have shown great potential as theranostic agents that enable both diagnostics and therapy. Conventional production methods lead to highly polydisperse microbubbles, which compromise the effectiveness of ultrasound imaging and therapy. Stabilizing microbubbles with surfactant molecules that can impart functionality and properties that are desirable for specific applications would enhance the utility of microbubbles. Here we generate monodisperse microbubbles with a large potential for functionalization by combining a microfluidic method and recombinant protein technology. Our microfluidic device uses an air-actuated membrane valve that enables production of monodisperse microbubbles with narrow size distribution. The size of microbubbles can be precisely tuned by dynamically changing the dimension of the channel using the valve. The microbubbles are stabilized by an amphiphilic protein, oleosin, which provides versatility in controlling the functionalization of microbubbles through recombinant biotechnology. We show that it is critical to control the composition of the stabilizing agents to enable formation of highly stable and monodisperse microbubbles that are echogenic under ultrasound insonation. Our protein-shelled microbubbles based on the combination of microfluidic generation and recombinant protein technology provide a promising platform for ultrasound-related applications.
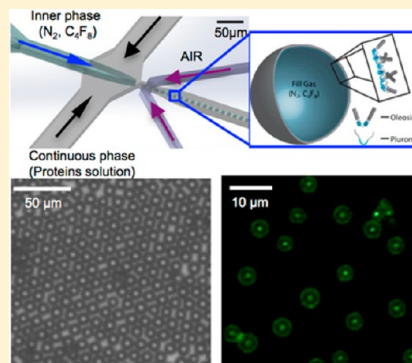
1. INTRODUCTION

Ultrasound imaging is one of the most inexpensive, safe, and commonly used diagnostic tools for imaging soft tissues and vasculature.[1] The use of microbubble contrast agents enables visualization of microvasculature which cannot be seen directly with Doppler ultrasound. Microbubbles composed of gaseous cores covered with stabilizing agents can drastically enhance the ultrasound signal because of their large compressibility, which leads to enhanced scattering of ultrasound.[2] The echogenicity of microbubbles coupled with their physical interactions with acoustic energy can also be used for triggered release of active agents or for conversion of acoustic energy to thermal energy to enable therapeutic applications. For example, recent studies have shown that the insonation of microbubbles with low-intensity ultrasound can lead to a localized temperature increase, which in turn disrupts tumor vasculature (also known as antivascular ultrasound therapy), enabling a minimally invasive procedure to disrupt cancerous tissues. These properties of microbubbles make them ideal candidates for theranostics; that is, the same microbubble agents can be used for diagnostics and therapeutic applications.[3]

Currently available commercial agents consist of polydisperse microbubbles with size distributed over a broad range of diameters. Studies have shown that the effectiveness of these agents can be significantly enhanced by making the size distribution narrow for molecular imaging and therapeutic

applications.[4−7] Although some methods to fractionate microbubbles to enhance the uniformity of size have been reported, these techniques inevitably lead to loss of significant fraction of bubbles.[4,8] Another important factor that significantly affects microbubble properties for ultrasound-related applications is the surfactant that is used to stabilize microbubbles. An approach to control the molecular structure and properties of these surfactants would be highly beneficial because their structure affects the surface functionality and the echogenicity of microbubbles. The generation of monodisperse microbubbles that are stabilized with surfactants that can be precisely designed and controlled would lead to microbubbles that have ideal functionality for ultrasound imaging and novel therapeutic approaches such as targeted drug delivery and antivascular ultrasound therapy (AVUST).[9−15]

In this study, we present a method to create stable protein-shelled microbubbles using a microfluidic flow focusing device that uses an air-actuated membrane valve, which enables the production of highly monodisperse sub-10 μm microbubbles. Although other studies have shown that monodispserse bubbles can be generated based on microfluidic techniques,[16−19] the size range of microbubbles that can be generated from such
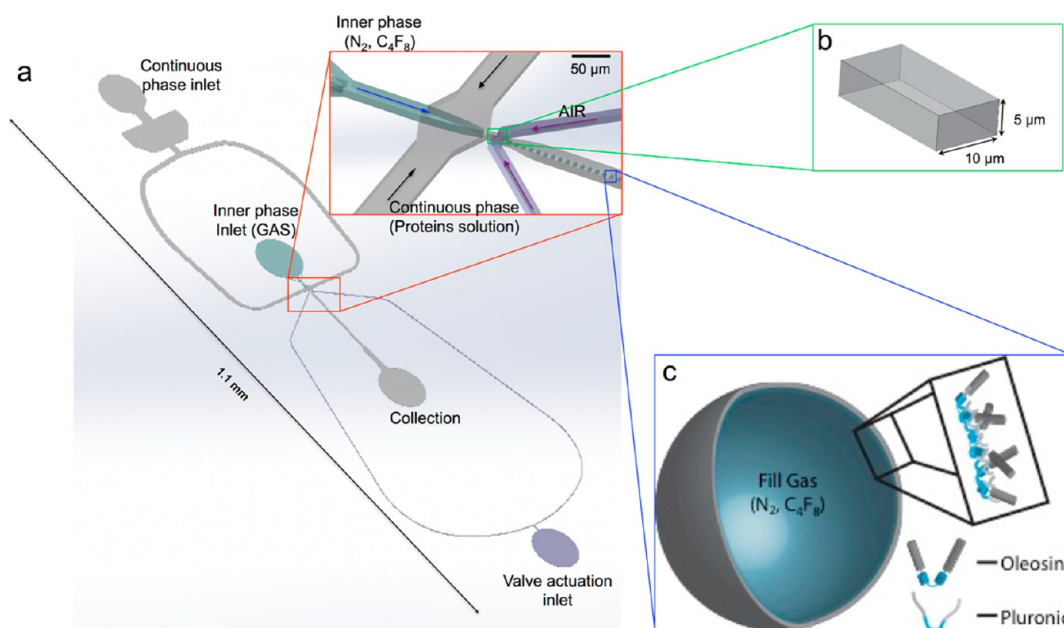
Figure 1. (a) Schematic illustration of a PDMS microfluidic device used to generate monodisperse microbubbles of different sizes. (b) Cross-sectional geometry of the nozzle (see Figure S1 for junction dimensions). (c) Schematic of a microbubble stabilized with a mixture of oleosin and $(PEO)_n$-$(PPO)_m$-$(PEO)_n$ triblock copolymer.

devices is somewhat limited. A method based on the dissolution of highly soluble gas such as CO_2 in a long microfluidic channel has shown to generate monodisperse bubbles of varying sizes.[20] A method that enables the formation of bubbles over a wide range of size without using soluble gas and long channels would provide a complementary method that can further expand the use of microfluidic techniques to generate monodisperse microbubbles. The air-actuated membrane valve enables precise control over the size of microbubbles while producing highly monodisperse microbubbles. To stabilize the microbubbles generated by the microfluidic technique, we use a novel mutant of the amphiphilic protein oleosin.[21,22] Unlike common proteins that have been used to stabilize microbubbles,[20,23,24] oleosin potentially provides versatility in imparting additional functionality via recombinant protein technology.[22,25] We demonstrate an example of such modularity by expressing and incorporating fluorescent oleosin into the microbubble shell. We demonstrate that careful tuning of the composition of the stabilizing agents is critical in the formation of highly stable and monodisperse microbubbles that are echogenic under ultrasound insonation.

2. MATERIALS AND METHODS

Microfluidic Device Fabrication. Microfluidic flow focusing devices with expanding nozzle design (Figure 1a) are fabricated using single layer soft lithography in poly(dimethylsiloxane) (PDMS).[26,27] Negative photoresist SU-8 2010 (Microchem, Newton, MA), thinned to a 3:1 ratio with SU-8 developer, is spin-coated onto a clean silicon wafer to a thickness of 5 μm and patterned to UV light through a transparency photomask (CAD/Art Service, Bandon, OR) using a Karl Suss MA4 Mask Aligner (SUSS MicroTec Inc., Sunnyvale, CA). To incorporate an air-actuated valve, we use single-layer membrane valves,[28] which exist in the same plane as the microfluidic channel, allowing us to fabricate the entire microfluidic device in a single layer mold. Sylgard 184 poly(dimethylsiloxane) (Dow Corning, Midland, MI) is mixed with cross-linker (ratio 12:1), degassed thoroughly and poured onto the photoresist pattern, and cured for 1 h at 65 °C to make the membrane highly compliant. The PDMS replica are peeled off the wafer and bonded to a PDMS membrane fabricated by spin-coating PDMS on a glass slide after oxygen plasma activation of both surfaces. Having a microchannel fully enclosed in PDMS allows for more efficient use of the valve membrane.

Gene Creation and Protein Expression. The sunflower seed oleosin gene is provided as a gift from Dr. Beaudoin at Rothamsted Research, Hampshire, England. Multiple rounds of PCR are used to create the oleosin gene 42-30G-63 and eGFP-30G-63. The genes are inserted into the expression vector pBamUK, a pET series derivative constructed by the Duyne Laboratory (SOM, Penn). Cloning details can be found in the Supporting Information. Mutants are confirmed through DNA sequencing prior to protein expression. pBamUK adds a 6-histidine tag to the C-terminus of the protein for IMAC purification. Protein is expressed in the *E. coli* strain BL21 DE3 (Stratagene) controlled by the lac promoter. Cultures are grown at 37 °C in Luria Bertani (LB) with kanamycin (50 μg mL^{-1}) until $OD_{600} \approx 0.7-0.9$. Protein expression is induced with isopropyl β-D-1-thiogalactopyranoside (IPTG) to a final concentration of 1.0 mM. Cells are harvested by centrifugation, and cell pellets are frozen at −20 °C prior to purification.

Protein Purification and Characterization. B-PER protein extraction agent (Fisher Scientific) is used for protein purification. 42-30G-63 is expressed in inclusion bodies whereas eGFP-42-30G-63 is expressed in the soluble fraction of the cell. 42-30G-63 is purified according to the B-PER protocol for inclusion bodies, and eGFP-42-30G-63 is purified according to the protocol for soluble proteins. Detailed purification information can be found in the Supporting Information. The concentration of purified protein is measured with a Nano-Drop 1000 (Thermo Scientific). Buffer exchange is completed with dialysis. All analysis is completed in PBS unless otherwise noted. To establish the purity of the proteins, SDS/PAGE gels are run on NuPAGE Novex 4−12% Bis-Tris mini gels (Invitrogen) in MES buffer. The gel is stained with SimplyBlue SafeStain (Invitrogen) following electrophoresis. The gel is destained overnight in water and imaged with a Kodak Gel Logic 100 imaging system. Protein molecular weight is confirmed with MALDI-TOF. Sample spots are created with 0.5 μL protein in 1× PBS and 0.5 μL of saturated sinapinic acid solution (50/50 acetonitrile/water + 0.1% TFE). Spectra are collected on an Ultraflextreme MALDI-TOF (Bruker, Billerica, MA) (see Figure S5 for eGFP spectra). To measure the protein secondary structure, far-UV CD spectra are collected at 25 °C on an AVIV 410 spectrometer (AVIV Biomedical Inc.) using a 1 mm quartz cell. Protein
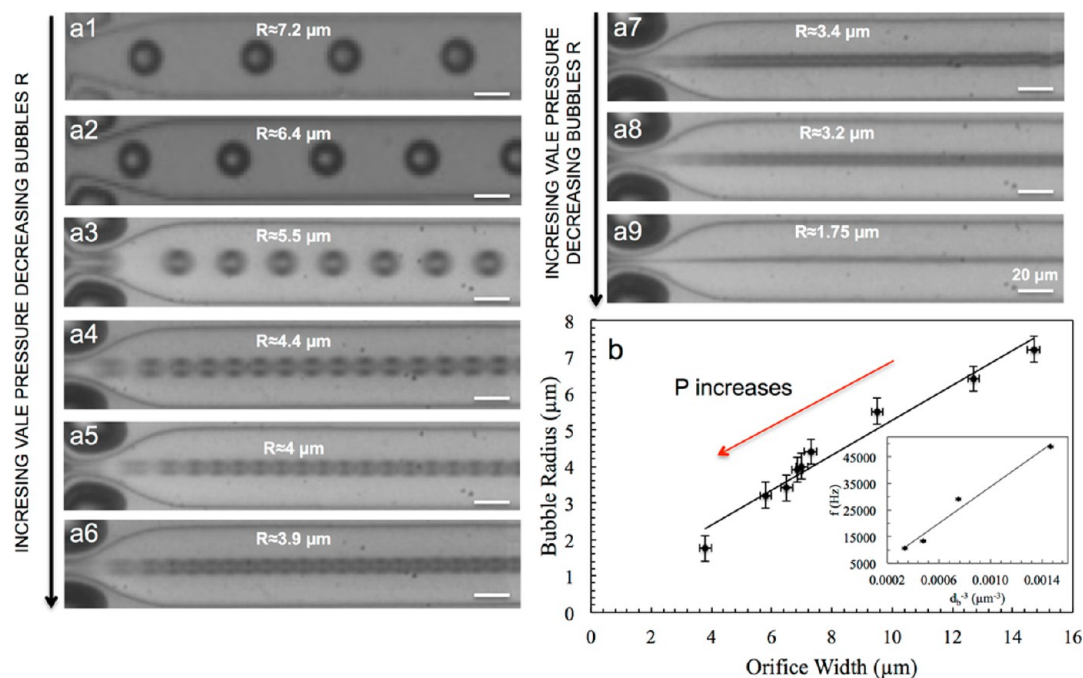
Figure 2. (a1−a9) Series of micrographs of the microfluidic device during the generation of microbubbles using a solution containing SDS at a concentration of 20 mg mL^{-1} in the aqueous phase. By changing the size of the nozzle, which is controlled by an air-actuated valve placed at the orifice, it is possible to generate uniform microbubbles of different sizes. (b) Effect of orifice width on the size of microbubbles. The inset shows the microbubbles generation frequency (f) vs volume of microbubbles (d_b^{-3}). The linear relationship between the two quantities indicates that the gas flow rates remains more or less constant under varying nozzle size.

concentration is 15 μM in 50 mM phosphate, 140 mM NaF. NaF is used to replace NaCl due to the strong absorbance of the Cl$^-$ ion.

Microbubbles Production and Characterization. The liquid phase containing the shell material consists of oleosin or a solution containing oleosin proteins and $(PEO)_{78}$-$(PPO)_{30}$-$(PEO)_{78}$ or $(PEO)_{100}$-$(PPO)_{65}$-$(PEO)_{100}$ diluted in phosphate-buffered saline (PBS) (pH 7.2, Sigma-Aldrich, St. Louis, MO). The components are mixed together to the desired concentration. Microbubbles are generated using liquid phases containing different combinations of the three components. The liquid phase consisting of oleosin and $(PEO)_n$-$(PPO)_m$-$(PEO)_n$ triblock copolymers at the optimal concentration dispersed in PBS is supplied to the device using a syringe pump (Harvard Apparatus PHD Ultra) at flow rates between 500 and 1000 μL h^{-1}. To connect the channels to syringes, polyethylene tubing with an i.d. of 0.38 mm and an o.d. of 1.09 mm (BB31695-PE/2, Scientific Commodities Inc, Lake Havasu City, AZ) is used. The gas phase consists of 99.999% pure nitrogen gas (N$_2$, GTS Welco, Richmond, VA) or octafluorocyclobutane (C$_4$F$_8$) (SynQuest Laboratories, Alachua, FL) supplied to the device using a pressure regulator (Type 700, ControlAir Inc., Amhrest, NH) at pressures between 15 and 20 psi. Polyethylene tubing with an i.d. of 0.86 mm and an o.d. of 1.32 mm (BB31695-PE/5, Scientific Commodities Inc, Lake Havasu City, AZ) is used connect the channel to the pressure regulator. The membrane valve is actuated using a dual-valve pressure controller (PCD-100PSIG-D-PCV10, Alicat Scientific, Tucson, AZ) at pressure between 0 and 40 psi.

Microbubbles are produced by first applying a small pressure to the gas inlet (2−4 psi) immediately followed by injecting the liquid phase at the desired flow rate (500−1000 μL h^{-1}). The gas pressure is then increased slowly until steady state of bubble generation is reached. Images of microbubbles production are captured using an inverted microscope (Nikon Diaphot 300) connected to a high speed Phantom V7 camera. For microbubbles that remain stable during generation and collection, long-term stability is characterized by collecting microbubbles at the air−water interface in 35 mm Petri dishes, acquiring images under an upright microscope (Carl Zeiss Axio Plan II) connected to a QImaging Retiga 2000R camera. Microbubbles

diameter variation over time is measured and images are analyzed using ImageJ (v 1.47v, NIH).

Fourier Transform Infrared (FT-IR) Spectroscopy. A Nicolet 8700 FT-IR spectrophotometer (Thermo Scientific) is used to obtain the FT-IR spectra of microbubbles and their constituent solutions on ZnSe windows (Phoenix Infrared, Lowell, MA). Samples are prepared by placing a small aliquot of solution on top of the window and are fully dried before measurements are performed. The spectra are taken between 5000 and 600 cm^{-1}, at 1.93 cm^{-1} wavenumber resolution.

Ultrasound Imaging. Microbubbles for ultrasonic imaging are collected and imaged directly in 16 mm membrane dialysis bag, which is prefilled with buffer solution and sealed at one end. After a desired amount of bubbles is collected, the tube is sealed at the other end, carefully avoiding formations of air pockets. The collected microbubbles are imaged using a clinical ultrasound scanner HDI 5000 (Phillips/ATL, Bothell, WA) which is equipped with a broadband high-frequency ultrasound transducer at 7−15 MHz. Grayscale B-mode images are acquired with a mechanical index (MI) of 0.37 and 0.47 with focus between 0.5−1.5 and 1−2 cm, respectively. Time gain compensation (TGC) is fixed throughout the experiments.

3. RESULTS AND DISCUSSION

For a variety of applications that involve microbubbles and ultrasound, the size distribution of microbubble agents drastically influences the efficacy of the image contrast enhancement and therapeutic methods. To enable formation of microbubbles with high monodispersity and, at the same time, tunable size, we use an expanding nozzle flow-focusing microfluidic device with a single-layer membrane valve at the orifice as schematically illustrated in Figure 1. A previous study has shown that the size of liquid emulsion droplets produced by a flow-focusing microfluidic device can be controlled by changing the size of the orifice via the actuation of the valve.[28] Likewise, this design gives us the flexibility to tune the size of gas microbubbles in the same chip without changing the

continuous phase or gas flow rates, by only changing the size of the orifice through the application of pressure to the valve. Furthermore, the use of the single-layer membrane valve overcomes the low resolution that is typically achieved by using polymeric photomasks (smallest feature ~10 μm).

For the initial testing of the microfluidic device to control the size of microbubbles, we use nitrogen gas and a common surfactant, sodium dodecyl sulfate (SDS, Sigma-Aldrich, St. Louis, MO), at a concentration of 20 mg mL^{-1} in the aqueous phase to stabilize microbubbles. We are able to produce monodisperse microbubbles with radius ranging from approximately 2 to 10 μm for several hours without changes in the bubble size. An advantage of this microfluidic device is that the size of microbubbles that can be generated from a single microfluidic device can be controlled over a wide range, unlike most flow-focusing microfluidic devices that have limited range of size control.[29,30] By increasing the pressure that is applied to the single-layer valve, we can control the size of the nozzle and, in turn, the size of microbubbles as shown in Figure 2. We observe that the diameter of the microbubbles, d_b, decreases linearly with the width of the nozzle, w_n. Interestingly, the microbubble generation frequency (f = the number of microbubbles generated per second) is inversely proportional to the volume of microbubbles as shown in the inset of Figure 2b ($f \sim d_b^{-3}$).[31] Such a trend indicates that the gas flow rate, calculated to be $Q_g \sim 62$ μL h^{-1} (σ^2 = 8.4 μL h^{-1}), remains more or less constant under varying nozzle size. The constant gas flow rate under varying nozzle width may be attributed to the change in the cross-sectional shape of the channel, from a horizontal slit to a square or hourglass shape. Although SDS enables the investigation of microfluidic device performance, microbubbles formed using SDS are not stable upon collection.

To produce stable microbubbles with high monodispersity, size tunability, and structural modularity, we use recombinant oleosin as the bubble shell material. Oleosin is a plant protein that stabilizes oil bodies in seeds.[21] The protein has a natural amphiphilic structure with N- and C-terminal hydrophilic arms and a central hydrophobic core containing a proline knot forcing the protein into a hairpin structure.[21,22,32,33] Oleosin has been used in various biotechnology and biomedical applications exploiting its amphiphilic properties.[34−38] In its native state, the solubility of oleosin in water is extremely low. Eliminating a large portion of the hydrophobic domain and removing the majority of the secondary structure in the protein backbone have been shown to yield a oleosin mutant that becomes highly soluble in water and naturally self-assembles into micelles.[25] The soluble oleosin mutant is named 42-30-63 defining the number of amino acids in each domain: the N-terminal hydrophilic arm, the central hydrophobic core, and the C-terminal hydrophilic arm, respectively. This molecule is produced by truncating the wild-type molecule without changes in the sequence of amino acids. The 42-30-63 oleosin mutant is further modified by inserting five glycines into the hydrophobic core (see Supporting Information for protein sequences) creating a mutant we refer to as 42-30G-63.[22] The protein is expressed in the *Escherichia coli* strain BL21 (DE3) with isopropyl β-D-1-thiogalactopyranoside (IPTG) induction. Protein is purified using immobilized metal affinity chromatography through a 6-histidine tag on the C-terminus of the protein, leading to highly purified products (Figure 3). Protein molecular weight is confirmed with SDS-polyacrylamide gel electrophoresis (SDS-PAGE) and matrix-assisted laser desorption/ionization-time-of-flight (MALDI-TOF) mass spectrosco-
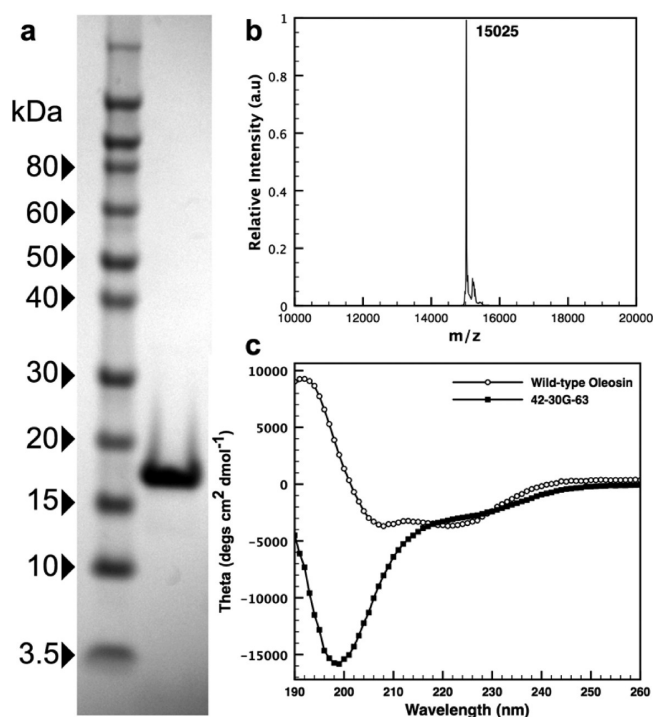

Figure 3. (a) SDS-PAGE gel showing >95% purity for 42-30G-63. (b) MADLI-TOF spectra confirming the molecular weight for 42-30G-63 (expected: 15 027; measured: 15 025). (c) Far-ultraviolet circular dichroism (UV CD) spectra of 42-30G-63 and wild-type oleosin. The former indicates a random coil structure.

py (Figure 3). The addition of the five glycines to the 42-30-63 mutant increases the protein expression, stability, and solubility while abolishing secondary structure, as shown by circular dichroism (Figure 3). In contrast, the CD spectra of wild-type (WT) oleosin shows β-sheet character as previously reported (see Supporting Information for detailed analysis).[22]

When we produce microbubbles using oleosin, at concentrations between 1 and 2 mg mL^{-1}, we can only stabilize bubbles with radius above 10 μm. During the generation of microbubbles with radii smaller than 10 μm, bubbles are observed to undergo coalescence within and outside of the microfluidic device (Figure S2). In addition, the relatively high surface tension between the liquid and the gas phases makes the generation of such microbubbles challenging, often resulting instability of microbubbles in the microfluidic device.

Interestingly, a number of microbubble systems that are currently being investigated (e.g., phospholipid-stabilized microbubbles) often have extra components such as poly-(ethylene glycol)-based surfactants such as amphiphilic triblock copolymers to enhance the microbubble stability and generation process. Thus, we add widely used poly(ethylene glycol)-*b*-poly(propylene glycol)-*b*-poly(ethylene glycol) triblock copolymers ($(PEO)_n$-$(PPO)_m$-$(PEO)_n$ where n and m denote the number of ethylene oxide and propylene oxide repeat units, respectively; these polymers are also known as Pluronic and Polxamer) to the oleosin solution to test whether the production of microbubbles can be facilitated.[39] We test two different types of $(PEO)_n$-$(PPO)_m$-$(PEO)_n$ triblock copolymers: $(PEO)_{100}$-$(PPO)_{65}$-$(PEO)_{100}$ and $(PEO)_{78}$-$(PPO)_{30}$-$(PEO)_{78}$. When we use a mixture containing 1−2 mg mL^{-1} oleosin and 5−20 mg mL^{-1} $(PEO)_{100}$-$(PPO)_{65}$-$(PEO)_{100}$ (average molecular weight 12 600), we are able to

consistently generate monodisperse microbubbles at the nozzle; however, these microbubbles undergo significant coalescence upon collection. In contrast, when we add $(PEO)_{78}$-$(PPO)_{30}$-$(PEO)_{78}$ (average molecular weight 8400) to oleosin solutions, we are able to generate microbubbles at the nozzle and very limited coalescence is observed upon collection. We find that the optimal concentration for stable microbubble formation requires an aqueous phase containing 1 mg mL^{-1} of oleosin and 10 mg mL^{-1} of $(PEO)_{78}$-$(PPO)_{30}$-$(PEO)_{78}$. $(PEO)_{78}$-$(PPO)_{30}$-$(PEO)_{78}$ is known to be more effective in stabilizing gas bubbles than $(PEO)_{100}$-$(PPO)_{65}$-$(PEO)_{100}$, which may explain the effectiveness of the former in facilitating the microbubble production.[40]

To further understand the possible role of $(PEO)_{78}$-$(PPO)_{30}$-$(PEO)_{78}$ in facilitating the formation of microbubbles and the role of oleosin in imparting long-term stability to microbubbles, we perform FT-IR spectroscopy of four different samples: pure oleosin, pure $(PEO)_{78}$-$(PPO)_{30}$-$(PEO)_{78}$, a mixture of oleosin and $(PEO)_{78}$-$(PPO)_{30}$-$(PEO)_{78}$ with the same composition as the solution used for microbubble generation (1:18 mole ratio), and microbubbles. FT-IR spectra remarkably show that the composition of microbubble shell is very different from that of the solution as shown in Figure 4. The concentration of oleosin
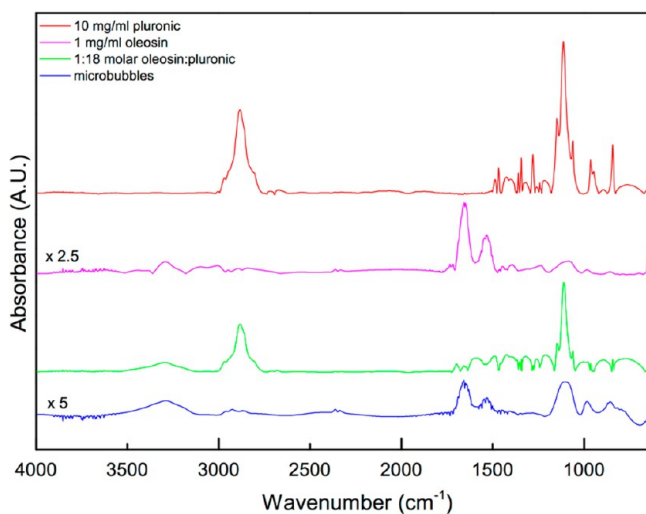
Figure 4. FTIR absorbance spectra of the components utilized to produce the bubbles and microbubbles. The spectra of pure oleosin and microbubbles are amplified by factors of 2.5 and 5, respectively, to clearly show the features.

present in the microbubble shell is significantly higher than that of the original solution used for microbubble generation, as evidenced by the prominent presence of peaks associated with pure oleosin in the microbubble spectrum (e.g., peaks found around 1535, 1650, and 3290 cm^{-1}). Although it is not straightforward to quantify the composition of the microbubble shell based on FT-IR, the comparison of the four spectra shows that oleosin seems to be the major species that is stabilizing microbubbles. These results suggest that $(PEO)_{78}$-$(PPO)_{30}$-$(PEO)_{78}$ present in the solution facilitates microbubble production by lowering the surface tension and rapidly covering the microbubbles upon breakup at the nozzle. Once microbubbles are generated and flow through the channel, oleosin starts to adsorb and possibly displace some of $(PEO)_{78}$-$(PPO)_{30}$-$(PEO)_{78}$ that are on the microbubble surface.

In the samples that are collected through polyethylene tubing, we typically observe that there are a small number of fairly large bubbles (>20 μm in diameter). Although the physical mechanism behind the appearance of these large bubbles is not known, their number fraction is extremely small, typically less than 1%. Interestingly, these large bubbles disappear completely approximately 24 h after collection, leaving behind a collection of highly monodisperse microbubbles as shown in Figure 5. We believe these large bubbles
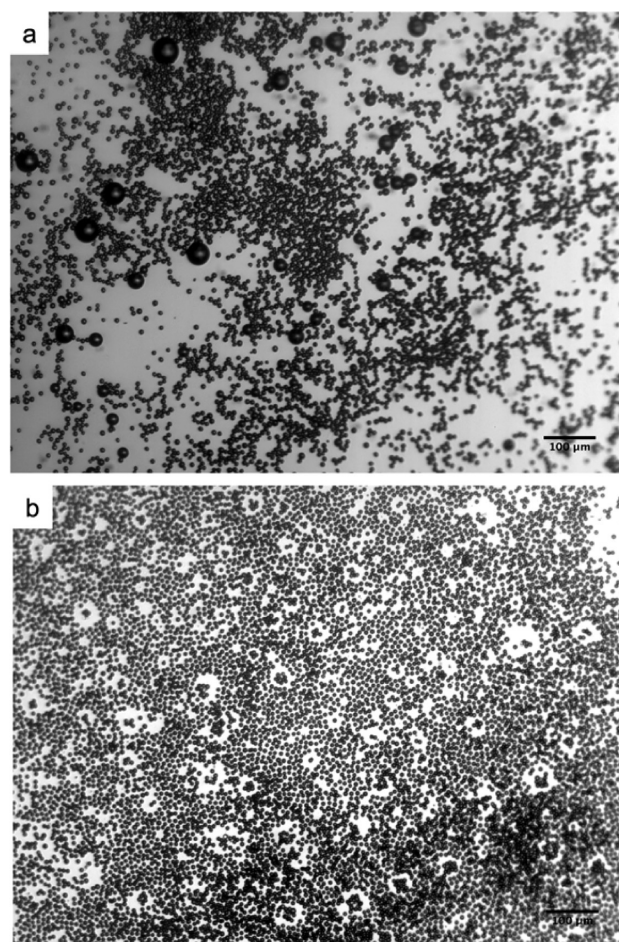
Figure 5. Micrographs of microbubbles produced using a solution containing 1 mg mL^{-1} oleosin and 10 mg mL^{-1} $(PEO)_{78}$-$(PPO)_{30}$-$(PEO)_{78}$. (a) A small number of large bubbles are present upon collection via plastic tubing. (b) Big bubbles disappear 24 h after collection, leaving monodisperse microbubbles.

dissolve over time. Since we do not see any major coalescence between microbubbles occurring within the PDMS microfluidic device, we believe these large bubbles likely form during transfer of the microbubbles from nozzle to a container via polyethylene tubing. Possibly, abrupt changes in dimensions and relative shear stress experienced by microbubbles between the PDMS device and the collection tube as well as the lower speed at which the microbubbles travel in the polyethyelene tube before being released in a Petri dish may lead to collision between bubbles and eventual coalescence. Another possibility is that these large bubbles have slightly different surface composition since they are observed to undergo dissolution when they are stored for an extended period, whereas the monodisperse bubbles that were originally generated at the

nozzle do not dissolve completely over a long period of time. Interestingly, we are able to collect highly monodisperse microbubbles without any large bubbles if we collect the produced bubbles straight into a well that is position in the same plane as the microfluidic channel (Figure 6). The high
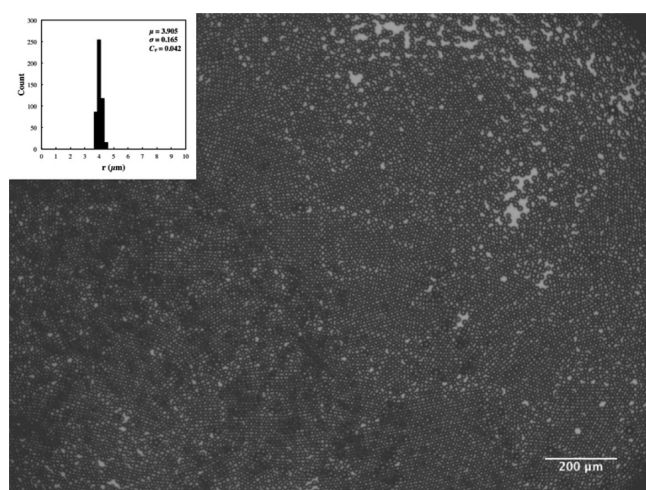

Figure 6. Micrograph of monodisperse microbubbles produced using a solution containing 1 mg mL^{-1} oleosin and 10 mg mL^{-1} (PEO)$_{78}$-(PPO)$_{30}$-(PEO)$_{78}$ and collected into a well in the PDMS device without the use of plastic tubing. The inset shows the microbubble size distribution for ∼500 microbubbles. μ, σ, and C_v in the inset represent the average (in μm), standard deviation (in μm), and coefficient of variation, respectively.

monodispersity of microbubbles is illustrated by their ability to pack into hexagonal array, which indicates that the coefficient of variation (C_v) is less than 5% around the average bubble size, consistent with our optical microscopy-based analysis. These results show that even small perturbations can lead to disruption of microbubbles that are generated using microfluidic devices, and extra care must be taken in collecting microbubbles for clinical applications since large bubbles in blood vessels can lead to serious problems such as embolism.

Microbubbles generated using the mixture of oleosin and (PEO)$_{78}$-(PPO)$_{30}$-(PEO)$_{78}$ (molar ratio of oleosin:triblock copolymer = 1:18) are remarkably stable once they are collected. When microbubbles are collected and stored in water (microbubbles reside at the air−water interface due to their buoyancy), microbubble radius decreases by about 13% during the first few days and eventually ceases to shrink further. These microbubbles remain stable at least for 4 weeks, and their size does not show any changes after 5 days as shown in Figure 7, suggesting that these microbubbles will not undergo dissolution even after 4 weeks. The stability of these microbubbles does not depend on whether N$_2$ or C$_4$F$_8$ is used as the gas phase. In contrast, microbubbles generated solely with (PEO)$_{78}$-(PPO)$_{30}$-(PEO)$_{78}$ do not exhibit such excellent stability. These results indicate that oleosin plays a critical role in stabilizing the shell of microbubbles, which likely consists of a mixture of oleosin and (PEO)$_{78}$-(PPO)$_{30}$-(PEO)$_{78}$, to prevent complete dissolution or coalescence of microbubbles upon their collection. Similar examples, in which shells suppresses the dissolution of microbubbles, have been observed in microbubbles that have been stabilized with other types of proteins, nanoparticles, or synthetic polymers.[20,41−61]
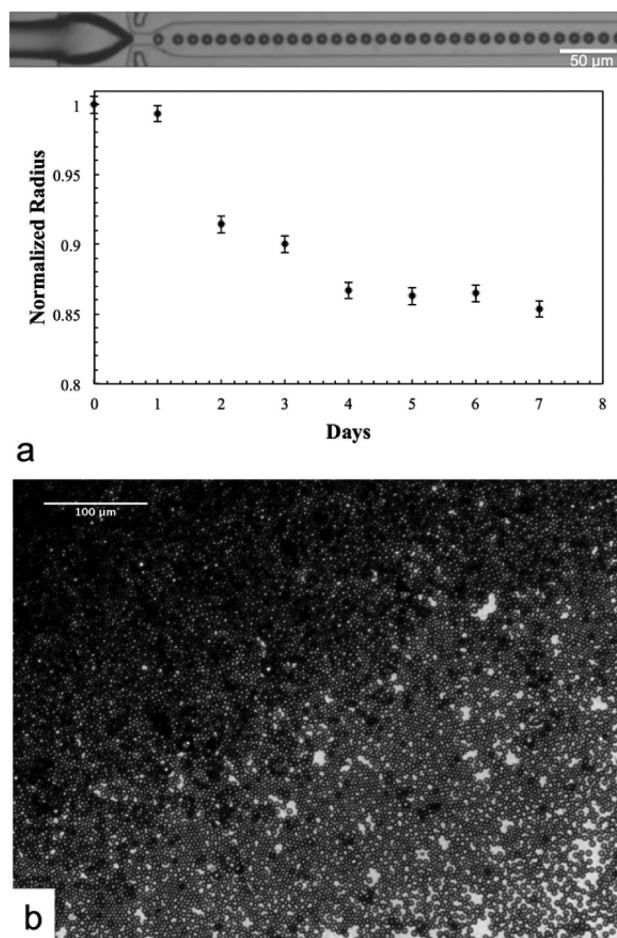

Figure 7. Micrographs showing microbubbles stability over time for microbubbles produced using a solution containing 1 mg mL^{-1} oleosin and 10 mg mL^{-1} (PEO)$_{78}$-(PPO)$_{30}$-(PEO)$_{78}$. (a) Size of microbubbles over 7 days. (b) Microscope images of 24 days after collection.

As discussed briefly above, one of the unique aspects of oleosin is that the molecular structure and thus the properties of the monolayer that contains this molecule can be engineered using recombinant protein technology. Recombinant protein technology allows for precise molecular engineering of proteins generated from microorganisms such as bacteria and thus can be used to generate oleosin species with different functionality and properties.[22] To demonstrate proof-of-principle that this molecule has such modularity, we express a green fluorescent protein mutant oleosin by fusing enhanced green fluorescent protein (eGFP) to the N-terminus of the 42-30G-63 oleosin. The modified oleosin genes are constructed using standard molecular biology techniques and cloned into the expression vector pBamUK. eGFP-funconalized oleosin is added to the aqueous phase during microbubble generation. It is evident that the microbubbles produced with the blend of the two oleosin species (pure at 1 mg mL^{-1}, mutant at 0.05 mg mL^{-1}) along with 10 mg mL^{-1} (PEO)$_{78}$-(PPO)$_{30}$-(PEO)$_{78}$ have the eGFP mutant species incorporated in the bubble shell, whereas the microbubbles generated without the eGFP mutant species do not show surface fluorescence (Figure 8). Also, fluorescence intensity is observed to be fairly uniform on the surface of the bubbles. Our results clearly indicate that that oleosin with different functionalities can be generated and incorporated into the microbubble shell and that oleosin distributes uniformly on the surface of microbubbles.
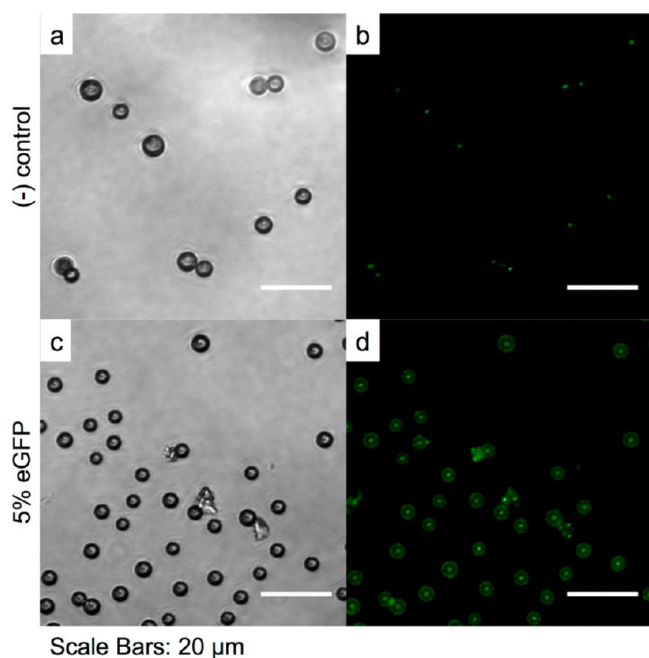
Figure 8. Confocal fluorescent microscopy images of bubbles produced with (a, b) oleosin and (c, d) with a blend containing the eGFP mutant. In both cases a solution containing 1 mg mL^{-1} oleosin and 10 mg mL^{-1} (PEO)$_{78}$-(PPO)$_{30}$-(PEO)$_{78}$ is used to produce microbubbles. Microbubbles are stored for 24 h before confocal microscopy is performed. These images are taken by focusing at the equatorial planes of the bubbles.[62]

Echogenicity measurements are carried out using microbubbles generated with a solution containing 1 mg mL^{-1} oleosin and 10 mg mL^{-1} (PEO)$_{78}$-(PPO)$_{30}$-(PEO)$_{78}$. We collect microbubbles directly in a ~3 cm long dialysis tubing with a diameter of 16 mm, which is sealed at one end and prefilled with PBS solution containing 10 mg mL^{-1} (PEO)$_{78}$-(PPO)$_{30}$-(PEO)$_{78}$. Microubbles are transferred directly into the dialysis tube from the PDMS device outlet using polyethylene tubing, which is submerged in the PBS solution. After collecting a desired amount of microbubbles, the tube is sealed on the other end to avoid introducing any air pockets and is stored in 50 mL centrifuge tubes filled with PBS solution containing 10 mg mL^{-1} (PEO)$_{78}$-(PPO)$_{30}$-(PEO)$_{78}$. The tube is kept on a spinning wheel rotating at 60 rpm to induce continuous motions of the microbubbles and more importantly to remove large bubbles that may have been collected. Since antivascular and other microbubble-based therapies are monitored using high-frequency ultrasound,[10,63] the echogenicity of the microbubbles is tested using a broadband high-frequency ultrasound transducer at 7−15 MHz in brightness mode (B-mode). The microbubbles are acoustically active along the entire length of the dialysis tube as shown in Figure 9. In contrast, a PBS solution containing 10 mg mL^{-1} (PEO)$_{78}$-(PPO)$_{30}$-(PEO)$_{78}$ without any microbubbles does not show any acoustic signal, indicating that the oleosin-stabilized microbubbles are highly echogenic. Microbubbles remain acoustically responsive 30 min after the initial measurement and even 1 week after the first measurement, showing nondetectable changes in the signal brightness (Figure 9). These results clearly indicate that these microbubbles stabilized with oleosin are highly stable and echogenic and thus could have significant potential for theranostic applications.
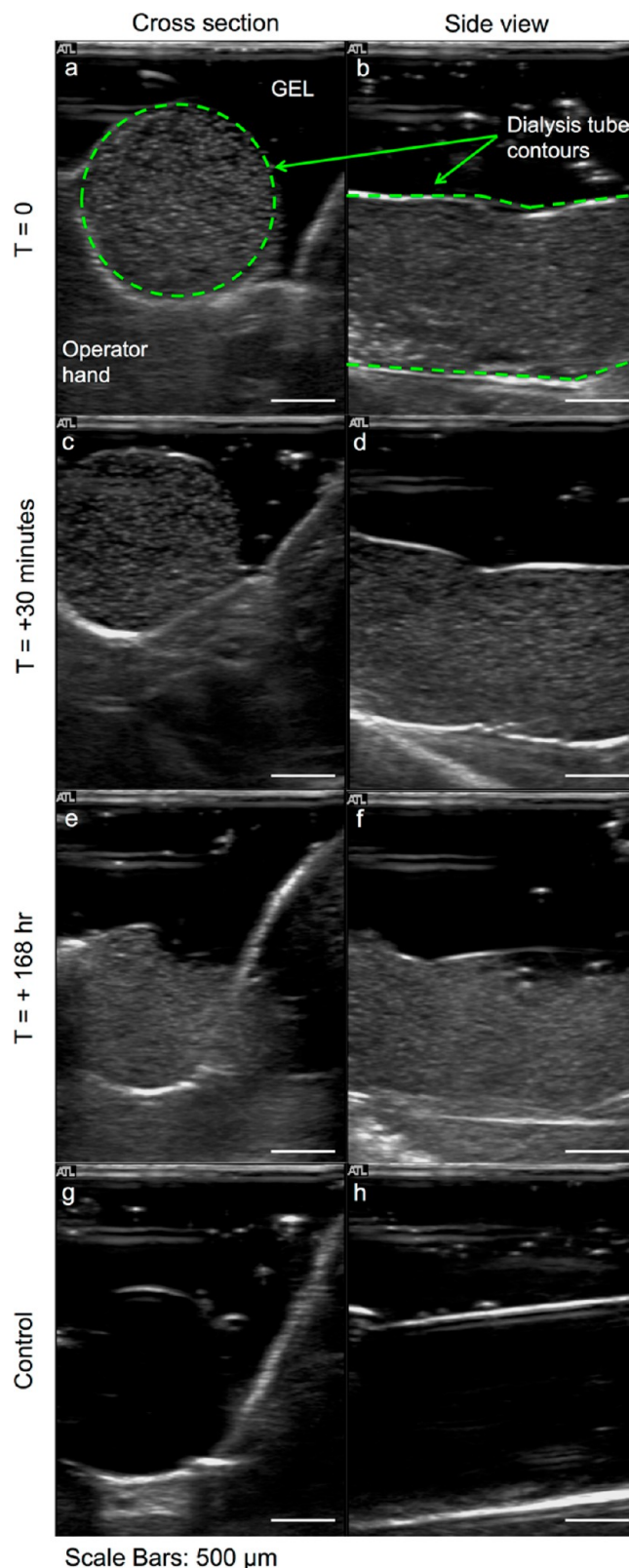

Figure 9. Ultrasound sonography images of C$_4$F$_8$ microbubbles generated with a solution containing 1 mg mL^{-1} oleosin and 10 mg mL^{-1} (PEO)$_{78}$-(PPO)$_{30}$-(PEO)$_{78}$. Ultrasound images of microbubbles (a, b) 1−2 h after generation and (c, d) 30 min and (e, f) 7 days after initial imaging. Ultrasound images of control samples are reported in panels g and h. The microbubbles have a radius of about 4 μm.

4. CONCLUSIONS AND OUTLOOK

We have shown that a recombinant mutant oleosin, in combination with a triblock copolymer, $(PEO)_{78}$-$(PPO)_{30}$-$(PEO)_{78}$, can be used to successfully produce stable and monodisperse microbubbles with high echogenicity. We demonstrate that the use of a PDMS microfluidic device with an air-actuated valve is an effective method to control the size of microbubbles while maintaining narrow size distribution. Microbubbles incorporating oleosin show high stability and can be further functionalized using recombinant protein technology, which we demonstrated by the incorporation of eGFP mutant oleosin into microbubbles. We envisage that the combination of microfluidic generation and oleosin-based stabilization of microbubbles will represent a promising platform for ultrasound-related applications. In particular, by functionalizing oleosin with specific targeting ligands via recombinant protein techniques,[36,37] it will be possible to enable localized microbubble-based ultrasound therapy. Also, by varying the molecular structure of oleosin (e.g., controlling the structure of hydrophobic domain), microbubble shells with different rheological properties could be generated.

■ ASSOCIATED CONTENT

Ⓢ Supporting Information

DNA sequence for 43-30G-63 and eGFP-43-30G-63, protein cloning method, protein purification protocol, microfluidic device channels and junction dimensions, micrograph of pure oleosin 43-30G-63 microbubbles, microscope image of microbubbles upon collection and after 7 days, SEM images of microbubbles, SDS-PAGE and MALDI TOF of eGFP-43-30G-63. This material is available free of charge via the Internet at http://pubs.acs.org.

■ AUTHOR INFORMATION

Corresponding Author

*E-mail: daeyeon@seas.upenn.edu (D.L.).

Present Address

F.E.A.: Department of Physics and Astronomy, University of Pennsylvania, Philadelphia, PA 19104.

Author Contributions

F.E.A. and K.B.V. contributed equally.

Notes

The authors declare no competing financial interest.

■ ACKNOWLEDGMENTS

■ REFERENCES

(1) Kiessling, F.; Fokong, S.; Koczera, P.; Lederle, W.; Lammers, T. Ultrasound microbubbles for molecular diagnosis, therapy, and theranostics. *J. Nucl. Med.* **2012**, *53*, 345−348.

(2) de Jong, N.; Cate, F. T.; Lancée, C.; Roelandt, J.; Bom, N. Principles and recent developments in ultrasound contrast agents. *Ultrasonics* **1991**, *29*, 324−330.

(3) Del Vecchio, S.; Zannetti, A.; Fonti, R. Nuclear Imaging in cancer theranostic. *Q. J. Nucl. Med. Mol. Imaging* **2007**, *51*, 152−163.

(4) Segers, T.; Versluis, M. Acoustic bubble sorting for ultrasound contrast agent enrichment. *Lab Chip* **2014**, *14*, 1705−1714.

(5) Talu, E.; Hettiarachchi, K.; Zhao, S.; Powell, R. L.; Lee, A. P.; Longo, L.; Dayton, P. A. Tailoring the size distribution of ultrasound contrast agents: possible method for improving sensitivity in molecular imaging. *Mol. Imaging* **2007**, *6*, 384−392.

(6) Streeter, J. E.; Gessner, R.; Iman Miles, I.; Dayton, P. A. Improving sensitivity in ultrasound molecular imaging by tailoring contrast agent size distribution: in vivo studies. *Mol. Imaging* **2010**, *9*, 87−95.

(7) Kaya, M.; Feingold, S.; Hettiarachchi, K.; Lee, A. P.; Dayton, P. A. Acoustic responses of monodisperse lipid-encapsulated microbubble contrast agents produced by flow focusing. *Bubble Sci. Eng. Technol.* **2010**, *2*, 33−40.

(8) Feshitan, J. A.; Chen, C. C.; Kwan, J. J.; Borden, M. A. Microbubble size isolation by differential centrifugation. *J. Colloid Interface Sci.* **2009**, *329*, 316−324.

(9) Wood, A. K.; Ansaloni, S.; Ziemer, L. S.; Lee, W. M.-F.; Feldman, C. M.; Sehgal, M. D. The antivascular action of physiotherapy ultrasound on murine tumors. *Ultrasound Med. Biol.* **2005**, *31*, 1403−1410.

(10) Wood, A. K.; Bunte, R. M.; Cohen, J. D.; Tsai, J. H.; Lee, W. M.-F.; Sehgal, C. M. The antivascular action of physiotherapy ultrasound on a murine tumor: role of a microbubble contrast agent. *Ultrasound Med. Biol.* **2007**, *33*, 1901−1910.

(11) Wood, A. K.; Bunte, R. M.; Price, H. E.; Deitz, M. S.; Tsai, J. H.; Lee, W. M.-F.; Sehgal, C. M. The disruption of murine tumor neovasculature by low-intensity ultrasounds comparison between 1- and 3-MHz sonication frequencies. *Acad. Radiol.* **2008**, *15*, 1133−1141.

(12) Wood, A. K.; Bunte, R. M. Acute increases in murine tumor echogenicity after antivascular ultrasound therapy a pilot preclinical study. *J. Ultrasound. Med.* **2009**, *28* (6), 795−800.

(13) Wood, A. K.; Schultz, S. M.; Lee, W. M.-F.; Bunte, R. M.; Sehgal, C. M. Antivascular ultrasound therapy extends survival of mice with implanted melanomas. *Ultrasound Med. Biol.* **2010**, *36*, 853−857.

(14) Goertz, D.; Karshafian, R.; Hynynen, K. Antivascular effects of pulsed low intensity ultrasound and microbubbles in mouse tumors. *IEEE Int. Ultrason. Symp.* **2008**, 670−673.

(15) Chin, C. T.; Raju, B.; Shevchenko, T.; Klibanov, A. Control and reversal of tumor growth by ultrasound activated microbubbles. *IEEE Int. Ultrason. Symp.* **2009**, 77−80.

(16) Gañán Calvo, A. M. Perfectly monodisperse microbubbling by capillary flow focusing: An alternate physical description and universal scaling. *Phys. Rev. E* **2004**, *69*, 027301.

(17) Anna, S. L.; Bontoux, N.; Stone, H. A. Formation of dispersions using "flow focusing" in microchannels. *Appl. Phys. Lett.* **2003**, *82*, 364−366.

(18) Garstecki, P.; Stone, H. A.; Whitesides, G. M. Mechanism for flow-rate controlled breakup in confined geometries: a route to monodisperse emulsions. *Phys. Rev. Lett.* **2005**, *94*, 164501.

(19) Dollet, B.; van Hoeve, W.; Raven, J.-P.; Marmottant, P.; Versluis, M. Role of the channel geometry on the bubble pinch-off in flow-focusing devices. *Phys. Rev. Lett.* **2008**, *100*, 034504.

(20) Park, J. I.; Tumarkin, E.; Kumacheva, E. Microbubbles loaded with nanoparticles: a route to multiple imaging modalities. *Macromol. Rapid Commun.* **2010**, *31*, 222−227.

(21) Huang, A. H. C. Oil bodies and oleosins in seeds. *Annu. Rev. Plant Physiol. Plant Mol. Biol.* **1992**, *43*, 177−200.

(22) Vargo, K. B.; Parthasarathy, R.; Hammer, D. A. Self-assembly of tunable protein suprastructures from recombinant oleosin. *Proc. Natl. Acad. Sci. U. S. A.* **2012**, *109*, 11657−11662.

(23) Suslick, K. S.; Grinstaff, M. W. Nonaqueous liquid filled microcapsules. *Polym. Prepr.* **1991**, *32*, 255−256.

(24) Cavalieri, F.; Ashokkumar, M.; Grieser, F.; Caruso, F. Ultrasonic synthesis of stable, functional lysozyme microbubbles. *Langmuir* **2008**, *24*, 10078−10083.

(25) Vargo, K. B.; Sood, N.; Moeller, T.; Heiney, P.; Hammer, D. A. Spherical micelles assembled from soluble recombinant olesoin mutants. *Langmuir* **2014**, *30*, 11292−11300.

(26) Xia, Y.; Whitesides, G. M. Soft lithography. *Angew. Chem., Int. Ed.* **1998**, *37*, 550−575.

(27) Dhanaliwala, A. H.; Chen, J. L.; Wang, S.; Hossack, J. A. Liquid flooded flow-focusing microfluidic device for in situ generation of monodisperse microbubbles. *Microfluid. Nanofluid.* **2013**, *14*, 457−467.

(28) Abate, A. R.; Romanowsky, M. B.; Agresti, J. J.; Weitz, D. A. Valve-based flow focusing for drop formation. *Appl. Phys. Lett.* **2009**, *94*, 023503.

(29) Tu, F.; Lee, D. Controlling the stability and size of double-emulsion-templated poly(lactic-co-glycolic) acid microcapsules. *Langmuir* **2012**, *28*, 9944−9952.

(30) Erb, R. M.; Obrist, D.; Chen, P. W.; Studer, J.; Studart, A. R. Predicting sizes of droplets made by microfluidic flow-induced dripping. *Soft Matter* **2011**, *7*, 8757−8761.

(31) This relationship is based on the bubble generation frequency when the width of the nozzle is larger than ∼7 μm. Below this value, the bubble generation frequency cannot be precisely determined.

(32) Alexander, L.; Sessions, R.; Clarke, A.; Tatham, A.; Shewry, P.; Napier, J. Characterization and modelling of the hydrophobic domain of a sunflower oleosin. *Planta* **2002**, *214*, 546−551.

(33) Peng, C.-C.; Lee, V. S. Y.; Lin, M.-Y.; Huang, H.-Y.; Tzen, J. T. C. Minimizing the central hydrophobic domain in oleosin for the constitution of artificial oil bodies. *J. Agric. Food Chem.* **2007**, *55*, 5604−5610.

(34) Bhatla, S.; Kaushik, V.; Yadav, M. Use of oil bodies and oleosins in recombinant protein production and other biotechnological applications. *Biotechnol. Adv.* **2010**, *28*, 293−300.

(35) Chang, M.-T.; Tsai, T.-R.; Lee, C.-Y.; Wei, Y.-S.; Chen, Y.-J.; Chen, C.-R.; Tzen, J. T. C. Elevating bioavailability of curcumin via encapsulation with a novel formulation of artificial oil bodies. *J. Agric. Food Chem.* **2013**, *61*, 9666−9671.

(36) Chiang, C.-J.; Lin, C.-C.; Lu, T.-L.; Wang, H.-F. Functionalized nanoscale oil bodies for targeted delivery of a hydrophobic drug. *Nanotechnology* **2011**, *22*, 415102.

(37) Chiang, C.-J.; Lin, L.-J.; Lin, C.-C.; Chang, C.-H.; Chao, Y.-P. Selective internalization of self-assembled artificial oil bodies by HER2/neu -positive cells. *Nanotechnology* **2011**, *22*, 015102.

(38) Peng, C.-C.; Chen, J. C.; Shyu, D. J.; Chen, M.-J.; Tzen, J. T. A system for purification of recombinant proteins in Escherichia coli via artificial oil bodies constituted with their oleosin-fused polypeptides. *J. Biotechnol.* **2004**, *111*, 51−57.

(39) Shih, R.; Bardin, D.; Martz, T.; Sheeran, P.; Dayton, P. A.; Lee, A. P. Flow-focusing regimes for accelerated production of mono-disperse drug-loadable microbubbles toward clinical-scale applications. *Lab Chip* **2013**, *13*, 4816−4826.

(40) Schmolka, I. R. Artificial skin I. Preparation and properties of pluronic F-127 gels for treatment of burns. *J. Biomed. Mater. Res.* **1972**, *6*, 571−582.

(41) Park, J. I.; Jagadeesan, D.; Williams, R.; Oakden, W.; Chung, S.; Stanisz, G. J.; Kumacheva, E. Microbubbles loaded with nanoparticles: a route to multiple imaging modalities. *ACS Nano* **2010**, *4*, 6579−6586.

(42) Park, J. I.; Nie, Z.; Kumachev, A.; Kumacheva, E. Small, stable, and monodispersed bubbles encapsulated with biopolymers. *Soft Matter* **2010**, *6*, 630−634.

(43) Dressaire, E.; Bee, R.; Bell, D. C.; Lips, A.; Stone, H. A. Interfacial polygonal nanopatterning of stable microbubbles. *Science* **2008**, *320*, 1198−1201.

(44) Lee, M. H.; Lee, D. Elastic instability of polymer-shelled bubbles formed from air-in-oil-in-water compound bubbles. *Soft Matter* **2010**, *6*, 4326−4330.

(45) Lee, M. H.; Prasad, V.; Lee, D. Microfluidic fabrication of stable nanoparticle-shelled bubbles. *Langmuir* **2010**, *26*, 2227−2230.

(46) Straub, J. A.; Chickering, D. E.; Church, C. C.; Shah, B.; Hanlon, T.; Bernstein, H. Porous PLGA microparticles: AI-700, an intra-venously administered ultrasound contrast agent for use in echocardiography. *J. Controlled Release* **2005**, *108*, 21−32.

(47) Eisenbrey, J. R.; Hsu, J.; Wheatley, M. A. Plasma sterilization of poly lactic acid ultrasound contrast agents: surface modification and implications for drug delivery. *Ultrasound Med. Biol.* **2009**, *35*, 1854−1862.

(48) Eisenbrey, J.; Burstein, O. M.; Wheatley, M. Effect of molecular weight and end capping on poly(lactic-co-glycolic acid) ultrasound contrast agents. *Polym. Eng. Sci.* **2008**, *48*, 1785−1792.

(49) Leodore, L.; Oum, K.; Lathia, J.; Wheatley, M. Surface modification of a polymeric contrast agent for cancer targeting. *IEEE Annu. Northeast Bioeng. Conf., 31st* **2005**, 142−143.

(50) El-Sherif, D. M.; Lathia, J. D.; Le, N. T.; Wheatley, M. A. Ultrasound degradation of novel polymer contrast agents. *J. Biomed. Mater. Res., Part A* **2004**, *68A*, 71−78.

(51) Narayan, P.; Wheatley, M. A. Preparation and characterization of hollow microcapsules for use as ultrasound contrast agents. *Polym. Eng. Sci.* **1999**, *39*, 2242−2255.

(52) Schrope, B.; Shen, P.; Wheatley, M. Polymeric systems for diagnostic ultrasound contrast agents. *Cosmet. Pharm. Appl. Polym.* **1991**, 371−384.

(53) Singhal, S.; Moser, C. C.; Wheatley, M. A. Surfactant-stabilized microbubbles as ultrasound contrast agents: stability study of Span 60 and Tween 80 mixtures using a Langmuir trough. *Langmuir* **1993**, *9*, 2426−2429.

(54) Borden, M.; Sirsi, S.; Hernandez, S.; Homma, S.; Kandel, J.; Yamashiro, D. Polyplex-microbubbles for improved ultrasound-mediated gene therapy. *J. Acoust. Soc. Am.* **2013**, *133*, 3409−3409.

(55) Geers, B.; De Wever, O.; Demeester, J.; Bracke, M.; De Smedt, S. C.; Lentacker, I. Targeted liposome-loaded microbubbles for cell-specific ultrasound-triggered drug delivery. *Small* **2013**, *9*, 4027−4035.

(56) Park, Y.; Luce, A. C.; Whitaker, R. D.; Amin, B.; Cabodi, M.; Nap, R. J.; Szleifer, I.; Cleveland, R. O.; Nagy, J. O.; Wong, J. Y. Tunable diacetylene polymerized shell microbubbles as ultrasound contrast agents. *Langmuir* **2012**, *28*, 3766−3772.

(57) Seo, M.; Gorelikov, I.; Williams, R.; Matsuura, N. Microfluidic assembly of monodisperse, nanoparticle-incorporated perfluorocarbon microbubbles for medical imaging and therapy. *Langmuir* **2010**, *26*, 13855−13860.

(58) Wan, J.; Stone, H. A. Lipid monolayer dilatational mechanics during microbubble gas exchange. *Langmuir* **2012**, *28*, 37−41.

(59) Chen, H.; Li, J.; Wan, J.; Weitz, D. A.; Stone, H. A. Gas-core triple emulsions for ultrasound triggered release. *Soft Matter* **2013**, *9*, 38−42.

(60) Zha, Z.; Wang, J.; Qu, E.; Zhang, S.; Jin, Y.; Wang, S.; Dai, Z. Polypyrrole hollow microspheres as echogenic photothermal agent for ultrasound imaging guided tumor ablation. *Sci. Rep.* **2013**, *3*, 2360.

(61) Garg, S.; Thomas, A. A.; Borden, M. A. The effect of lipid monolayer in-plane rigidity on in vivo microbubble circulation persistence. *Biomaterials* **2013**, *34*, 6862−6870.

(62) A bright spot in the center of each microbubble, we believe, is due to an artifact of confocal microscopy. Similar bright spots have been observed and attributed to an artifact due to reflection in previous reports (Masters, B. R.; Paddock, S. W. Confocal bioimaging the living cornea with autofluorescence and specific fluorescent probes. *Bioimaging and Two-Dimensional Spectroscopy*, 1990; *Proc. SPIE 1205*, 164. Masters, B. R. Confocal microscopy of the eye. *New Methods in Microscopy and Low Light Imaging*, 1989; *Proc. SPIE 1161*, 350.

(63) Sehgal, C. M.; Cary, T. W.; Arger, P. H.; Wood, A. K. W. Delta projection imaging on contrast-enhanced ultrasound to quantify tumor microvasculature and perfusion. *Acad. Radiol.* **2009**, *16*, 71−78.